

# Sink vs. tilt penetration into shaken dry granular matter: the role of foundation

G. Sánchez-Colina,<sup>1</sup> A. J. Batista-Leyva,<sup>2</sup> C. Clément,<sup>3</sup> E. Altshuler,<sup>1</sup> and R. Toussaint<sup>3</sup>

<sup>1</sup>*Group of Complex Systems and Statistical Physics,  
Physics Faculty, University of Havana, 10400 Havana, Cuba*

<sup>2</sup>*Instituto Superior de Tecnologías y Ciencias Aplicadas (InSTEC). Salvador Allende  
esq. Luaces s/n. Plaza de la Revolución CP 10400. POB 6163. La Habana,  
Cuba and Group of Complex Systems and Statistical Physics,  
Physics Faculty, University of Havana, 10400 Havana, Cuba*

<sup>3</sup>*Institut de Physique du Globe de Strasbourg (IPGS),  
Ecole et Observatoire des Sciences de la Terre (EOST),  
University of Strasbourg/CNRS, 67084 Strasbourg, France*

(Dated: May 26, 2016)

We study the behavior of cylindrical objects as they sink into a dry granular bed fluidized due to lateral oscillations, in order to shed light on human constructions and other objects. Somewhat unexpectedly, we have found that, within a large range of lateral shaking powers, cylinders with flat bottoms sink vertically, while those with a “foundation” consisting in a shallow ring attached to their bottom, tilt besides sinking. The latter scenario seems to dominate independently from the nature of the foundation when strong enough lateral vibrations are applied. We are able to reproduce the observed behavior by quasi-2D numerical simulations, and the vertical sink dynamics with the help of a Newtonian equation of motion for the intruder.

PACS numbers: 45.70.-n, 45.70.Mg, 07.05.Tp, 96.15.Wx, 07.07.Df

## INTRODUCTION

The Kocaeli earthquake occurring on August 17, 1999 affected in various ways many constructions in the city of Adapazari, Turkey. Following observers, some buildings sank vertically into the soil, others tilted as shown on Fig. 1, and some even suffered lateral translation over the ground [1–3]. This case illustrates well the diversity of damage that earthquake fluidization of soils may cause to man-made structures [4].

Liquefaction in the ground may be originated dynamically, by shear waves released during earthquakes, generating cyclic shear stresses that lead to the gradual build-up of pore water pressure. The shaking produced by seismic events is a trigger for extensive liquefaction, as was observed recently in Belgium [5].

Ground fluidization [6, 7] has been investigated in different kinds of media like sand [7], dry granular soils [8] and sediments [9]. Of immediate interest for engineering and for the geosciences is to understand how man-made structures such as buildings, and massive rocks laying on granular soils respond to fluidization associated to seismic waves.

Granular matter itself displays a variety of puzzling phenomena [10–23], but during the last decade or so, our understanding of the dynamics of objects penetrating into granular media has advanced quickly [24–37]. While laterally shaken granular beds have received a certain degree of attention [38, 39], the performance of objects initially laying on the surface of a granular bed submitted to lateral shaking has been rarely studied [40–42].

In this paper we perform systematic experiments asso-



FIG. 1. Tilted building after the Izmit Earthquake, Aug 17th, 1999, Adapazari village, Turkey. Picture: Courtesy of Mustapha Meghraoui, IPGS.

ciated to the latter scenario, which may help understanding the performance of human constructions and rocks laying on granular beds during earthquakes. In particular, using a cylinder as a simplified model for buildings or rocks, we study its settling dynamics on a granular bed submitted to lateral vibrations. Somewhat unexpectedly, we have found that, within a large range of lateral shaking powers, cylinders with flat bottoms sink vertically, while those with a “foundation” consisting in a shallow ring attached to their bottom, tilt besides sinking. The latter scenario seems to dominate independently from the nature of the foundation when strong enough lateral vibrations are applied. Quasi-2D simulations were also performed mimicking the experiments. The settling dynamics of the simulated intruders, with or without foundation

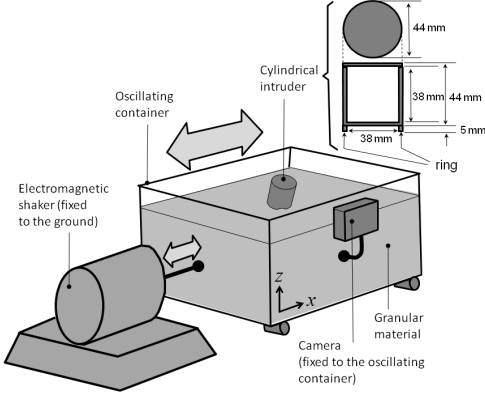


FIG. 2. Experimental setup. At the upper right, we have illustrated the intruder consisting in a cylinder with ring.

reproduces quite well the corresponding experimental results. We also developed a model that reproduces well the sinking dynamics and gives a qualitative explanation of the tilting process.

## EXPERIMENTAL

The penetration experiments were performed on a granular bed contained into a test cell of approximately  $25 \times 25 \times 25 \text{ cm}^3$  filled with Ugelstad spheres of non expanded polystyrene with a density  $1.05 \text{ g/cm}^3$ , and diameter  $140 \mu\text{m}$  (monodisperse within a 1 percent), type Dynoseeds ©, produced by Microbeads, Norway. The box was horizontally shaken at different amplitudes ( $A$ ), and a frequency ( $f$ ) of 5.0 Hz (a value commonly found in seismic waves), using a TIRA TV51120 shaker, type S51120, see figure 2. The maximum amplitude of oscillations allowed by the shaker corresponds to an acceleration of  $\approx 12.2 \text{ m/s}^2$ .

Two types of intruders were used in the experiments: (a) a hollow 3D printed cylinder of 44 mm diameter, 44 mm height (external dimensions), and 5 mm thick walls, and (b) the same cylinder with a ring of 5 mm height and 3 mm thickness glued to its bottom (illustrated in the upper right corner of Fig. 2). Intruders (a) and (b) will be called “No-ring” and “Ring”, respectively, from now on. Their masses were adjusted with ballast in such a way that their densities matched the average effective density of the granular medium, which was measured as  $0.43 \text{ g/cm}^3$ . As far as the ballast used has a density near the effective density of the granular material, it was almost evenly distributed inside the cylinder. Note that, using a flat bottom cylinder and a ring-like bottom cylinder, we are modifying the “foundation” of our intruder.

A digital camera *Hero 2* made by GoPro was fixed to the electromagnetic shaker, in such a way that it could take a video of the sinking process from an oscillating

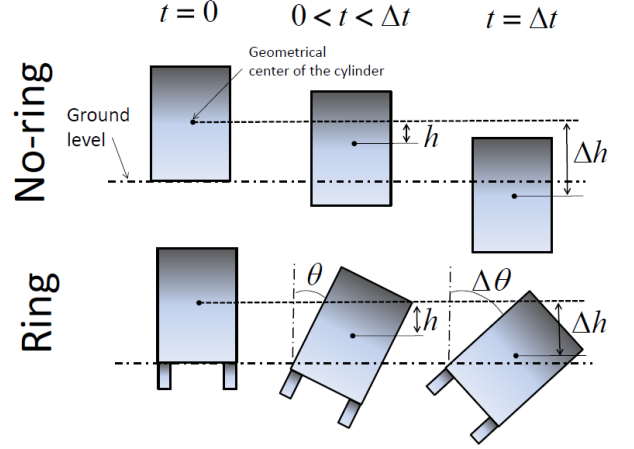


FIG. 3. Sketch of sinking and tilting processes. The top row illustrates the sinking process of a No-Ring cylinder in three moments during the experimental interval from  $t = 0$  to a final time  $t = \Delta t$ . The bottom row shows the same temporal sequence for a Ring cylinder, which tilts in addition to sink.

reference frame locked to the test cell, as proposed in [42]. This method allowed a much better quality of the cylinder’s images, and made easier their digital processing. Videos were taken at a maximum rate of 120 frames per second, with a resolution of  $1920 \times 1080$  pixels.

The images were processed as follows. We first converted the videos to image sequences in \*.jpg format, and cropped each picture, excluding irrelevant space. Then, the images were binarized through an appropriate threshold. Using the tool *regionprops* from *MatlabR2014a*, we identified and assigned coordinates to several bright marks we had glued to certain points of the cylindrical intruder. The coordinates of the marks were used to calculate the position of the intruder’s geometrical center and inclination relative to the vertical in each picture. In some experiments where the sinking was particularly big, it was difficult to obtain the tilt angle, since part of the marks sank below the level of the sand surface, and they were impossible to follow. In such cases the upper border of the cylinder was identified using the Matlab’s tools *find* and *bwtraceboundary*, and then fitted to a polynomial using the function *polyfit*. The fit was used to find the inclination. In the case of experiments ending in a very inclined position, the reference to calculate the inclination was the cylinder’s corner above the sand surface, that was identified as the intersection of the two polynomial fits of the upper and one lateral borders of the cylinder.

As the cylinder vibrates due to the vibration of the box, it is difficult to determine the final position, particularly when there is a big tilting. Then, in order to determine the sinking depth and tilting, we observe in the videos the onset of a cyclic movement of a reference point in

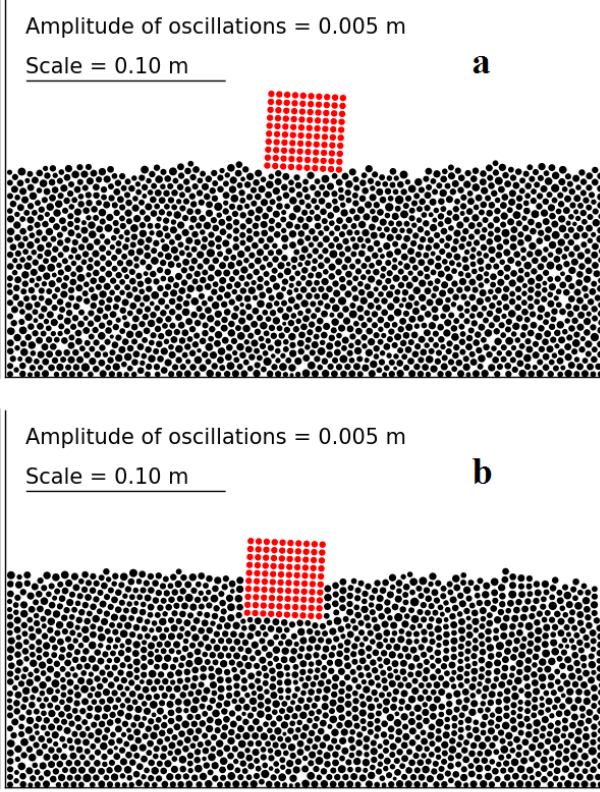


FIG. 4. (color online) Initial (a) and final (b) positions of No-ring intruder in a typical quasi-2D simulation using a frequency of 5 Hz (amplitude included in the graph).

the cylinder. Once this situation was reached, the final position could be measured in the frames filmed after the shaker was stopped.

The experimental protocol can be described as follows: (I) preparing the granular medium by stirring it evenly with a long rod, (II) gently depositing the cylinder in the upright position on the free surface of the granular bed, (III) turning ON the camera, (IV) switching ON the shaker after setting the desired frequency and amplitude (V) turning OFF the shaker and the camera after the penetration process had visibly finished.

In Fig. 3 we define the main parameters describing the sinking process of a No-ring cylinder (upper row), and the tilting and sinking of a Ring cylinder (bottom row), during the experimental lapse, defined as  $\Delta t$ . As the figure indicates, in the following we will call  $h$  the penetration of the geometrical center at a time  $t$  and  $\Delta h$  the final penetration at time  $t = \Delta t$ . It is important to note that both magnitudes are defined as the vertical displacement of the geometrical center of the cylinder (without taking into account the ring).

We also explored the observed phenomenology through numerical simulations. They were based on a discrete element method code (DEM) for the computation of gran-

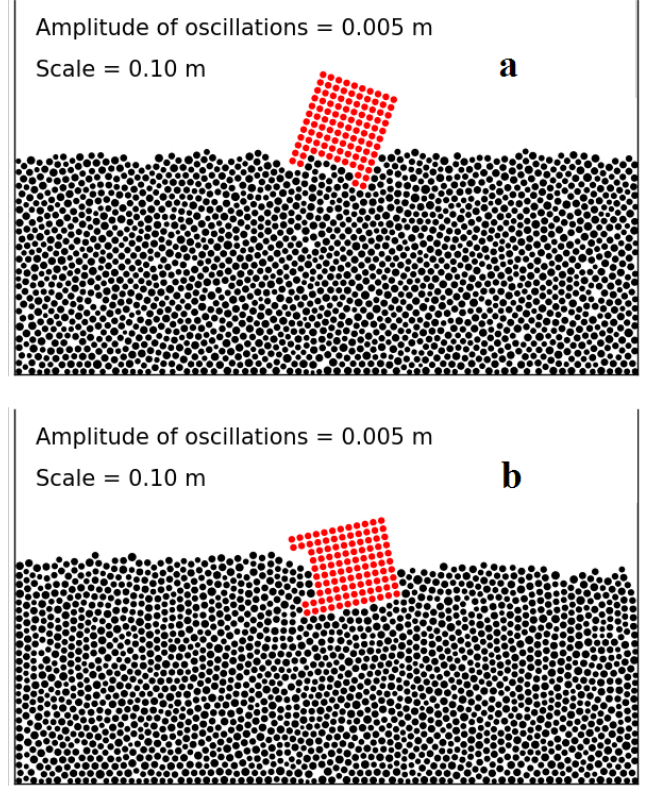


FIG. 5. (color online) Initial (a) and final (b) positions of Ring intruder in a typical quasi-2D simulation using a frequency of 5 Hz (amplitude included in the graph).

ular systems [18, 20, 22, 43, 44]. We modeled a quasi-2D granular medium, made of spheres of diameter 4 mm monodisperse within a 1 percent to avoid the effect of crystallization, and a thickness of 0.2 mm. The numerical medium contains 2000 particles, filling a virtual space of 30 cm width and 10 cm height. The code calculates the position and rotating angle of each sphere derived from the different forces applied on it. The friction coefficient  $\mu$  is taken as 0.3. To approach the experimental conditions, we simulate particles of density  $1.05 \text{ g/cm}^3$ .

We created two intruders made of cohesive particles. One is a square of 40 mm side, made of 100 particles placed in a quasi-2D square arrangement, which simulates the No-ring intruder of the experiments. The second one is another square of 40 mm side attached to two small feet made of 4 particles each, mimicking the cross section of the ring attached to the bottom of the intruder. The particles density of the spheres which form the intruders is  $1 \text{ g/cm}^3$ , and the porosity of the intruders is 0.21 percent, so the intruder density is  $0.78 \text{ g/cm}^3$ , i.e., approximately the same effective density of the quasi-2D granular medium.

Once our granular medium is created, we place the intruder 1 mm above the medium. We let it drop and



settle until the whole medium reaches equilibrium. Then, we apply a horizontal oscillation of different amplitudes and a frequency of 5 Hz to the walls of the medium and compute the time evolution of the position and tilting angle of the intruder.

Figures 4 and 5 show the initial and final positions of both types of intruders in two typical runs. Fig. 4 indicates that the No-ring cylinders almost do not tilt, while in Fig. 5 is obvious the wide inclination of a Ring one.

## RESULTS AND DISCUSSION

### Sink vs. tilt penetration

Figure 6(a) shows the time variation of the sinking depth for selected values of the adimensional acceleration  $\Gamma = A(2\pi f)^2/g$  (where  $g = 9.81 \text{ m/s}^2$  is the gravitational acceleration and  $A(2\pi f)^2$  is the horizontal peak acceleration of the sand box) for No-ring cylinders. It is easy to see that the penetration of the No-ring cylinders follows a common pattern for all the accelerations. A first process of fast sinking is followed by a slow creep. Only the penetration depth increases with  $\Gamma$ . In this figure we do not show the total creep process, due to its long duration. As the height of the cylinder is 44 mm, it is possible to check from Fig. 6(a) that, for an adimensional accelerations of 1.24, the cylinder sinks completely.

Figure 6(b) is similar to the previous one, only measurements were performed with Ring cylinders.

The general features of both graphics are very similar, but there is a difference, that will be better observed in the following figures: the adimensional acceleration at which the cylinder sinks completely in the medium is bigger for the Ring cylinders than for the No-ring ones. We could have a glimpse of why it occurs if we analyze Fig. 6(c), that presents the time evolution of the tilting angle for a Ring cylinder. Let us analyze, for instance, the curve for the highest adimensional acceleration shown in the figure ( $\Gamma = 1.24$ ). In the first second the inclination angle reaches a value around  $25^\circ$ , resulting in the increase of the effective size of the intruder, with the corresponding increase of the forces impeding the sinking process (we will further develop these ideas below). All in all, it explains why the Ring cylinder sinks less than the No-ring one.

Another important difference is that the sinking and tilting dynamics of Ring cylinders is more irregular than that of the No-ring ones. It is easy to understand, if we imagine the tumbling process. Firstly the intruder gets an initial inclination along one of the two possible directions, due to the horizontal acceleration provoked by the shaker, that breaks the symmetry in a non predictable way. When the inclination appears, the gravity produces an additional torque that increases it. But, as the granu-

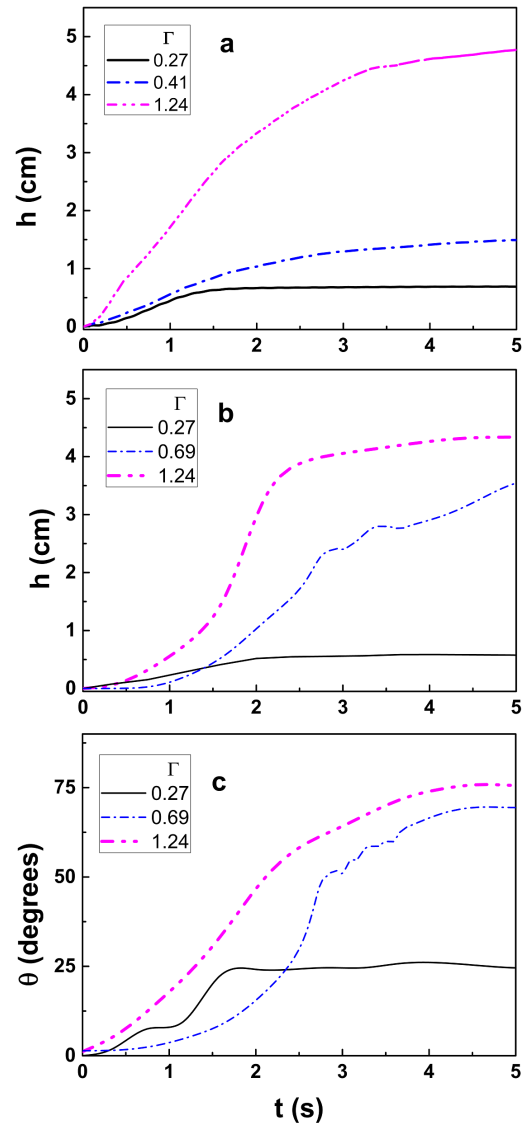


FIG. 6. (color online) Time evolution of penetration depths and tilt angles. Time dependence of the penetration depth of a No-ring cylinder (a), the penetration depth of a Ring cylinder (b) and the tilting angle of a Ring cylinder (c), for different adimensional accelerations. The long-time creep process is not completely shown. The tilting angle of No-ring cylinders is not displayed, due to the fact that it oscillates around angles not larger than  $5^\circ$  relative to the vertical direction

lar medium oscillates, the torque applied on the cylinder by the granular medium changes its orientation, provoking an oscillation in the emerged part of the intruder, so the tilting angle and the height of the center of mass relative to the surface of the granular medium also oscillate. This is illustrated in Fig. 6(b) and (c), even after being submitted to an averaging process.

In general, No-ring cylinders tend to sink vertically as the granular soil is fluidized by horizontal shaking, while cylinders with rings tend to tilt. Figure 7 quanti-

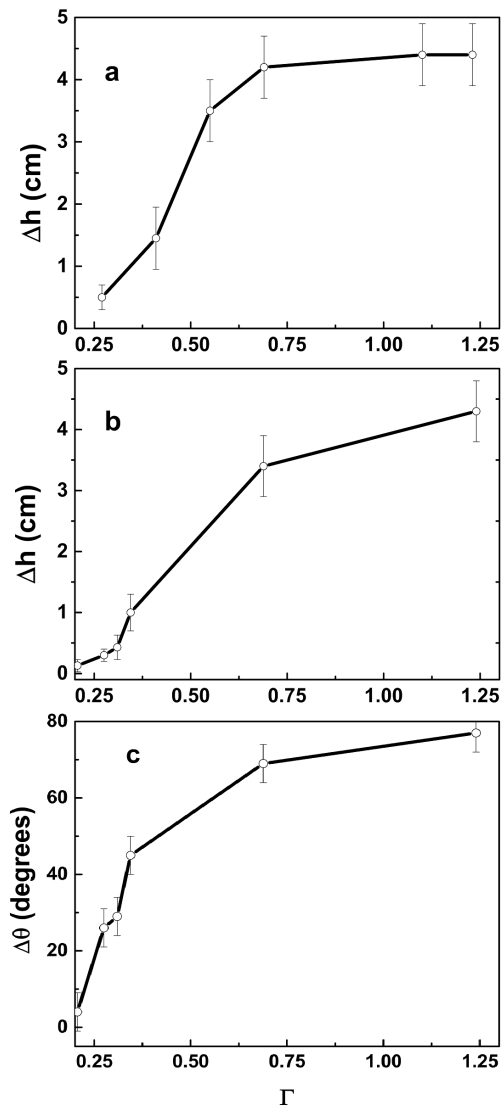


FIG. 7. Sinking and tilting: heights and angles. Final vs. initial sink heights for No-ring cylinders (a) and for Ring cylinders (b). Tilt angles for Ring cylinders (c). Tilt angles of No-ring cylinders are not shown for the same reasons of the previous figure.

fies the differences between the initial and final stages of the process, for almost all the range of accelerations our experimental setup was able to reach.

Figure 7(a) shows sink data for No-ring cylinders. As can be seen, for adimensional accelerations up to  $\Gamma = 0.27$ , there was no significant penetration of the intruder into the granular bed. Vertical penetrations started to increase significantly above  $\Gamma \approx 0.3$ , reaching a plateau around  $\Gamma \approx 0.75$ . At the plateau, the cylinder has sank completely, but stays “floating” into the fluidized granular medium, as expected for an object isodense relative to it.

In Fig. 7(b) the sinking process of the Ring cylinders is summarized. Differently from the previous case,

the plateau is not observed for the range of accelerations recorded. Note that as far as the depth reached at  $\Gamma \approx 1.2$  is approximately 4.4 cm (the height of the cylinder), for bigger accelerations this would also be the final penetration, so we can safely imply that the plateau appears at higher accelerations for that type of cylinders. But even at the highest accelerations, there is always a small part of the cylinder above the ground level.

Figure 7(c) shows the tilt data for Ring cylinders. No significant tilting is observed for  $\Gamma$  smaller than approximately 0.25. With the increase of the adimensional accelerations, the cylinder significantly tilts, increasing abruptly the tilting angle with  $\Gamma$ , until saturation starts at  $\Gamma \approx 0.75$ . As was stated in the figure caption, we do not show the tilting angle of No-ring cylinders, because it is always smaller than  $5^\circ$ , with a random distribution of values around the vertical direction.

Figures 7(b) and (c) are closely related, because they are two descriptions of the same process: the motion of Ring cylinders into the granular medium, that includes both sinking and tilting. The fact that at the accelerations shown in this figure the plateau in the sinking depth is barely reached while for the tilting angle it is, could be explained by the increase of the friction of the intruder with the granular medium when the tilting angle increases. Then, at  $\Gamma \approx 0.75$  the intruder has approximately reached its maximum inclination, but is not completely submerged in the medium. An increase in the acceleration does not increase significantly the angle, because the resulting torque has diminished due to the influence of both sinking and tilting, but the increase in fluidization helps further sinking, until most of the cylinder is submerged, reaching the plateau.

The overall behavior in Fig. 7(a) can be understood taking into account the experimental results in Ref. [40]. When the system is submitted to lateral shaking, a “solid” layer is formed, starting at a depth  $h_f$  that depends on the adimensional acceleration  $\Gamma$ . For accelerations in the range we used,  $h_f$  varies almost linearly with  $\Gamma$  (see Fig. 3(a) in Ref. [40]), so we can write

$$h_f(\Gamma) = \alpha(\Gamma - \Gamma^*); \Gamma > \Gamma^* \quad (1)$$

where  $\Gamma^*$  is the onset of fluidization and  $\alpha$  is the slope of the linear dependence. If  $\Gamma \leq \Gamma^*$  the depth of the fluidized layer is zero.

According to reference [45],  $\Gamma^*$  can be taken as proportional to the friction coefficient  $\mu$  between the cylinder and the granular medium. So in this experiments we can approximate  $\mu \approx 0.3$ , that is the value we use for the simulations. They also conclude that the final depth of intrusion depends on isostasy, and on the severity of shaking. It can be entirely determined by isostasy, when the shaking completely unjam the medium and suppresses the average friction around the intruder.

Then, at low values of  $\Gamma$  the granular media is not fluidized, and the cylinder almost does not sink (merely

5 mm at  $\Gamma = 0.27$ ; see Fig. 7(a)). At accelerations above the fluidization threshold, the cylinder sinks until it gets in contact with the solid layer. The larger is the acceleration, the deeper is that layer, so the bigger is  $\Delta h$ . But as soon as the solid layer appears at a depth larger than the cylinder's height, it does not sink further: instead, it “floats” due to isodensity with the sand, so a plateau is reached.

The strong differences in the dynamics of No-ring and Ring cylinders within the adimensional acceleration range  $0.3 \leq \Gamma \leq 1.3$  can be rationalized qualitatively as follows. The bottom of the cylinders with no ring offers small tangential friction to the sand surface during the first moments of the fluidization process (when they are on top of the granular surface), which implies a small torque between the horizontal friction at the bottom and the horizontal inertial force that can be represented at the center of mass of the cylinder. So, the cylinder keeps its vertical position since the beginning of the process, and just sinks vertically into the sand due to the action of gravity.

Differently from No-ring cylinders, the basement of a Ring one is firmly settled in the granular material, so, when an acceleration is imposed by the shaker, a significant torque appears, arising from the force exerted by the sand on the ring, and the inertial force at the cylinder's center of mass, forcing it to tilt. Moreover, the presence of the ring prevents the free flow of sand near the bottom of the cylinder, which makes more difficult its vertical sinking: as the sink time increases, the torque caused by horizontal forces has “better possibilities” to tilt the cylinder.

Two additional factors influence the sinking dynamics of this type of intruder: firstly, the tilting process changes the effective size of the cylinder, changing the drag and hydrostatic forces (in a way that will be analyzed below), which contributes to a Brazil nut like effect: isodense large particles tend to rise during shaking. Additionally, when the inclination is high, most of the cylinder could be inside the sand, and it starts to float, preventing further tilting.

Comparing figures 7 (a) and (b) it is possible to see that when the cylinder tilts it reaches a smaller final depth than when it sinks without tilting, for similar adimensional accelerations. It supports the idea that the inclination of the body increases the resistance forces acting on it.

Figure 8(a) reports the time interval needed by No-ring cylinders to penetrate into the granular material, from the moment when the vibration was turned ON, until they find their new equilibrium position. If we compare this figure with figure 7(a), a main difference can be appreciated: the plateau is now reached at a higher acceleration. Anyway, both the sinking depth and sinking times increase monotonically with the increase of  $\Gamma$  and saturate for accelerations at which the cylinder is eventually

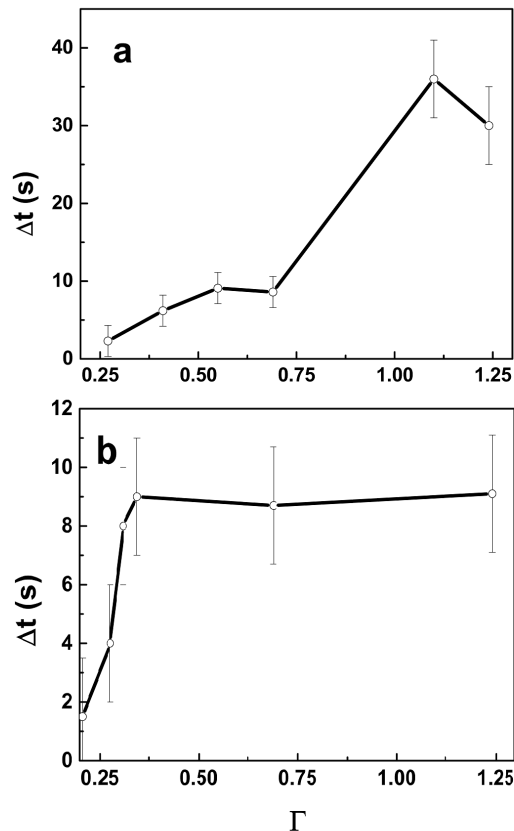


FIG. 8. Sinking times for No-ring cylinders (a) and tilting times for Ring cylinders (b). Sinking times for Ring cylinders are almost equal to their tilting times, so they are not shown.

completely immersed in the material.

Figure 8(b) shows a different tendency: the Ring cylinders tilt very fast, reaching a final inclination long before the final depth of the No-ring ones is reached. A careful inspection of the videos shows that No-ring cylinders sink fast during the first few seconds, but dramatically slow down during the penetration of the last millimeters, resulting in long sinking times. On the other hand, when Ring cylinders end the tilting process, they do not significantly sink further, perhaps due to the increase of the friction and buoyancy. That is why we do not show the sinking times of Ring cylinders: they are almost equal to the times shown in Fig. 8(b).

When we compare this figure with Fig. 7(c), an important difference is easily appreciated: though the tilt angle increases monotonically with  $\Gamma$ , the tilt times increase abruptly, and then saturate. That behavior could be related with the fact that, for small accelerations, the tilting process occurs slowly, but the tilting angle is small. By contrast, for bigger accelerations the tilting angle is larger, but the tilt occurs at bigger angular velocities, giving almost constant tilting times ( $\Delta t = \theta/\omega$ ).

### A phenomenological Newtonian model

In order to formulate a model to describe analytically the sinking process, let us consider the forces acting on the cylinder. As soon as the shaking starts, if the adimensional acceleration is above the threshold, the upper part of the granular bed is fluidized, and the intruder sinks.

Let us assume that the cylinder just sinks vertically, and let us name the vertical downward axis as  $z$ . The force balance on the intruder can be written as

$$m\vec{a} = m\vec{g} + \int (-P)\hat{n}dS + \int \sigma_s \cdot \hat{n}dS \quad (2)$$

where  $P$  is the pressure,  $\sigma_s$  the shear stress tensor,  $\hat{n}$  is the vector normal to the intruder's surface, and the integrals run over the boundary of the intruder that is inside the granular material. Assuming a hydrostatic pressure profile, we can write:

$$P = \int_0^h \rho(z')gz'dz' \quad (3)$$

where  $h$ , as previously, is the depth reached by the cylinder below the surface of the granular medium. In Eq. (3) we have made explicit that the density of the material varies with depth. Let us assume that it varies as a power law between zero and the density of the solid layer,  $\rho_{sl}$ , that is reached at a depth  $h_f$ :

$$\rho(z') = \rho_{sl} \left( \frac{z'}{h_f} \right)^p \quad (4)$$

where  $p \in [0, 1]$ .

By combining (4) and (3) and integrating, we find the hydrostatic buoyancy force acting on the cylinder with a length  $h$  under the (average) level of the granular bed, as:

$$\int (-P)\hat{n}dS = -\frac{\rho_{sl}Sg}{(p+1)h_f^p} h^{p+1} \hat{h} \quad (5)$$

where  $S$  is the characteristic area of the intruder cross section, and  $\hat{h}$  is a unit vector pointing downwards. It is easy to see that the buoyancy force depends on the volume submerged into the granular medium.

Assuming that inertial forces can be neglected, the shear stress component goes as

$$\int \sigma_s \cdot \hat{n}dS = -D\gamma v \hat{h} \quad (6)$$

where  $\gamma$  has the dimensions of a viscosity,  $D$  is the characteristic size of the cross section of the intruder,  $v$  is

its sinking speed and  $\hat{h}$  is the unit vector pointing downwards [46, 47]. By substituting Eq. (5) and Eq. (6) into Eq. (2), and only recovering the modular values, we get:

$$m \frac{d^2 h}{dt^2} + D\gamma \frac{dh}{dt} + \frac{\rho_{cs}Sg}{(p+1)h_f^p} h^{p+1} = mg \quad (7)$$

Before solving Eq. (7) we will assume that the sink velocity is constant, which follows quite well the behavior during the fast sink regime, as seen in Fig. 8 (*i.e.*, we neglect the inertial term). So,

$$\frac{dh}{dt} + \frac{\rho_{sl}Sg}{D\gamma(p+1)h_f^p} h^{p+1} = \frac{mg}{D\gamma} \quad (8)$$

which can be written as

$$\frac{dh}{dt} + ah^{p+1} = b \quad (9)$$

The definitions of  $a$  and  $b$  are easily deduced comparing Eqs. (8) and (9).

Equation (9) has analytical solutions if  $p = 0$  or  $p = 1$ , which correspond to the extreme cases of constant density and a linear density profile with depth, respectively. The solutions are

$$h(t) = \frac{b}{a}(1 - e^{-at}) \quad (10)$$

if  $p = 0$ , and

$$h(t) = \sqrt{\frac{b}{a}} \tanh(\sqrt{abt}) \quad (11)$$

if  $p = 1$ .

It is easy to see that both expressions correspond to an exponential growth that saturates.

Figure 9 shows the experimental results (continuous line) obtained for an adimensional acceleration  $\Gamma \simeq 0.3$ . It is possible to see in more detail the initial fast sinking process, followed by the slow creep. Fig. 9 also shows the fitting of equations (10, 11) to experimental data. Even the simplified Eq. (10) reproduces well the main features of the sinking process.

It is almost impossible to determine experimentally the exact density profile. But we do not need to know it in order to validate our model, if we use the following rationale. Firstly, we fit Eqs. (10, 11) to the experimental data and obtain the values of  $a$ ,  $b$  that correspond to  $p = 0$  ( $a(p=0)$ ,  $b(p=0)$ ) and  $p = 1$  ( $a(p=1)$ ,  $b(p=1)$ ). Let us assume that  $a$  and  $b$  vary linearly with  $p$  between the extremes values which were obtained from the fitting process. For an intermediate value of  $p$  (say,  $p_1$ ) we can calculate the corresponding values of  $a(p_1)$  and  $b(p_1)$ .

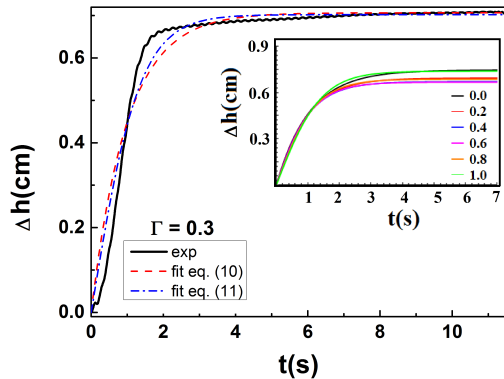


FIG. 9. (color online) Time dependence of sinking depth for the No-ring cylinder from experiment, compared with that determined from Eqs. (10, 11). The inset shows the solutions of Eq. (7) for different values of  $p$  (see text).

With them, we can in turn determine the constants of Eq. (7). Then, we solve this equation numerically. This procedure is repeated for values of  $p$  between 0 and 1, with a step of 0.1.

The inset in Fig. 9 shows some of the numerical solutions for the values of  $p$  in the legend. The main conclusion is that the density profile has small influence on the first (and most important) part of the sinking process. Of course, the final depth is influenced by the value of  $p$ , but due to experimental uncertainties, it is almost impossible to choose any particular value.

Let us now study the influence of the values of  $p$  in the quality of the fit of the solution of Eq. (7) to the experimental data. For doing this we note that the values of  $a$  and  $b$  in Eq. (10) can be easily obtained from the experiments. Considering Eq. (9) in the first moments of motion, as  $h$  is small,  $h'(t) \simeq b$ , so  $b$  can be evaluated as the initial slope. As at large times  $h(t) \sim h_{eq}$  ( $h_{eq} = \Delta h$  if  $h(0) = 0$ ) then  $a = b/h_{eq}^{p+1}$ . Then solving Eq. (7) for a given value of  $b, p, a(p)$  and naming the result  $h_{mod}$ , the best value of  $p$  arises from the minimization:

$$\min \sum_{i=1}^N (h_{mod}(t, p) - h_{exp}(t))^2 \quad (12)$$

where  $h_{exp}(t)$  are the experimental values of  $h$ .

The result for  $\Gamma \leq 1.0$  is indifferent to  $p$ : the fit is equally good no matter which is the value of  $p \in [0, 1]$ . For  $\Gamma = 1.24$  there are differences in the quality of fits for different  $p$ , but Eq. (12) gives a minimum for  $p = 0$ , so, we will assume  $p = 0$  in the following. Then, Eq. (7) becomes:

$$m \frac{d^2 h}{dt^2} + D \gamma \frac{dh}{dt} + \frac{\rho_{sl} S g}{h_f} h = mg \quad (13)$$

that can be taken as the simplest equation of motion that describes the vertical sink dynamics of our cylinders. It is worth noticing that Eq. (13) reproduces quite closely the results reported in Fig. 8, and can be used to explain the vertical sinking of Ring-cylinders while tilting, as we will see below.

Before that, it is instructive to compare equation (13) for a granular bed fluidized by shaking, with that proposed in [28] to describe the penetration of an intruder into ultra-light granular material that eventually behaves like a fluid medium even in the absence of shaking. The equation proposed in [28] reads as:

$$m \frac{d^2 h}{dt^2} = mg - \eta \left( \frac{dh}{dt} \right)^2 - \kappa \lambda \left( 1 - e^{-\frac{h}{\lambda}} \right) \quad (14)$$

Firstly we will analyze the last term of Eq. (14) which is related to Janssen's pressure. If we were applying this equation to our system, we should have taken into account that the shaking promotes the destruction of the force chains. That is equivalent to assume a very big  $\lambda$ , which yields a pressure force of the form  $\kappa \lambda (z/\lambda) = \kappa z$ , as proposed earlier in [26]. Comparing with Eq. (13) we see that the depth-dependent terms in both equations are similar, provided that

$$\kappa = \frac{\rho_{sl} S}{h_f} g \quad (15)$$

(notice that the linear relation of  $\kappa$  with  $g$  has been demonstrated experimentally in [34]).

However, there is an important difference in the “viscous drag” terms between equations (13) and (14): in the first, the velocity is linear, while it is squared in the second. Indeed, we cannot reproduce our experimental sink process if we insert in Eq. (13) a squared velocity term. However, the difference can be justified by the fact that the sink velocities in our shaken-bed experiment are much smaller than those observed in the penetration experiments reported in [28] and [34].

Now we concentrate again in the interpretation of our experimental results. In order to understand the tilting dynamics, it is useful to note that, when applying Eq. (13) to a tilted cylinder, the values of both  $D$  and  $S$  change. The reason is that when we calculate the surface integral, the result will be proportional to the cylinder's immersed volume. As the cylinder tilts, the immersed surface increases more than in the case of sinking without tilting, so the drag force is bigger in the former case. Considering, for instance, the situation represented in the lower row of Fig. 3, when the cylinder sinks a distance  $\Delta h$ , the surface increases as the inverse of  $\cos \theta$  (of course, other intruder geometries may follow different laws).

To test it, let us assume a simplified model: the increase factor of  $S$  and  $D$  is proportional to the characteristic size of the cross section of the cylinder projected



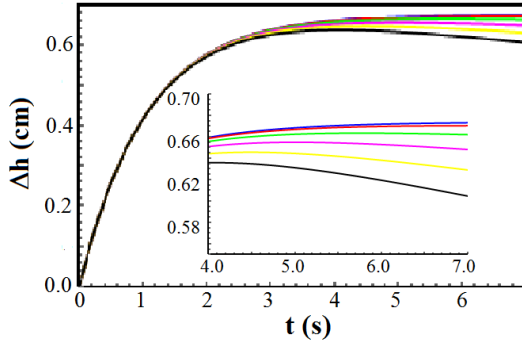


FIG. 10. (color online) Time dependence of sinking depth as calculated solving numerically Eq. (13) considering the variation of  $S$  and  $D$  provoked by tilting (see text). Upper curve is for  $\theta_{max} = 0$  while the lower one is for  $\theta_{max} = \pi/3$ . Between them,  $\theta_{max}$  varies in steps of  $\pi/15$ . The inset shows the last three seconds.

on the horizontal plane, i.e., it is proportional to the inverse of  $\cos \theta$ . Then, instead of  $D$  and  $S$ , we will solve Eq. (13) using  $D/\cos \theta(t)$  and  $S/\cos \theta(t)$ , where  $\theta(t)$  is a function that grows from zero to the maximum angle  $\theta_{max}$  reached by the cylinder, mimicking Fig. 6(c).

The consequences can be seen in Fig. 10. While in the beginning the sinking process in all situations occurs with the same dynamics, as the cylinder approaches the final angle, the behavior changes, been the final depth larger for the situations corresponding to low tilting.

The upper curve, calculated for  $\theta = 0$  coincides with the upper curve in the inset of Fig. 9 (calculated for  $p = 0$ ). Subsequent curves are calculated for values of  $\theta_{max}$  varying in steps of  $\pi/15$ , the lowermost curve corresponds to  $\theta_{max} = \pi/3$ . As the inclination of the cylinder increases, both the buoyancy and the viscous drag do. The effect of these factors on the sinking process of Ring cylinders was already noted in Fig. 6(b): an immediate consequence is the decrease of the sinking depth (for a given  $\Gamma$ ), compared with that of the No-ring ones, which can be easily observed in the experiments. In the inset it is possible to deduce that, for the larger angles, a small decrease in the depth is observed, suggesting the influence of a Brazil nuts like effect.

In spite of the simplifications assumed, it is worth noting that the basic differences between Fig. 7 (a) and (b) are reproduced by our model.

Finally, there is another element that was also not considered in our model: as the container shakes horizontally, it is equivalent to a horizontal drag that changes periodically its direction. According to [48], it creates an additional lift force, and also a dependence of the drag force with depth, which, of course, must influence the detailed penetration dynamics of the Ring cylinders.

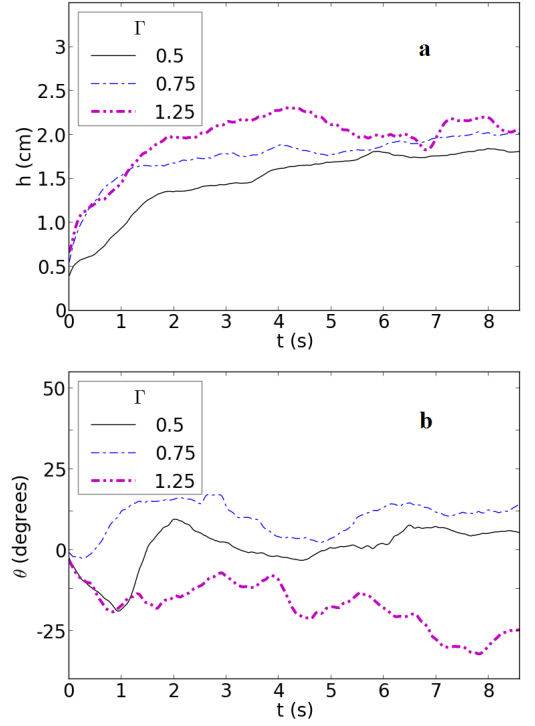


FIG. 11. (color online) Time dependence of sinking depth (a) and tilting angle (b) for a simulated quasi-2D No-ring cylinder.

### Quasi-2D numerical simulations

In figure 11 we can see the behavior of the quasi-2D No-ring intruder for three different adimensional accelerations. The same accelerations have been applied to a medium containing the simulated Ring intruder, see Fig. 12.

Regarding the vertical sinking, we do not observe major changes between Ring and No-ring intruders. We can notice that they sink less than in the experiments, which may be related with the dimensionality of the simulation relative to the real experiment. Quasi-2D granular media allow less choices of readjustment than in 3D: they are easily jammed, which makes it more difficult for an object to sink. Moreover, the size ratio of the intruder over the particles is 15 times smaller in the simulations than in the experiments (experiments:  $44\text{mm}/0.280\text{mm} = 150$ ; simulations:  $40\text{mm}/4\text{mm} = 10$ ), which means that if one particle is stuck under the intruder during the simulations, it will slow down the intruder significantly more than if the particle were 15 times smaller. In addition, since the numerical intruder is made out of particles of the same size as the particles of the medium, it may be rougher than the experimental intruder.

For the tilting, we find that the presence of foundation at the bottom of the intruder causes a large tilting. Indeed, for the shaking with No-ring, the intruder tilting

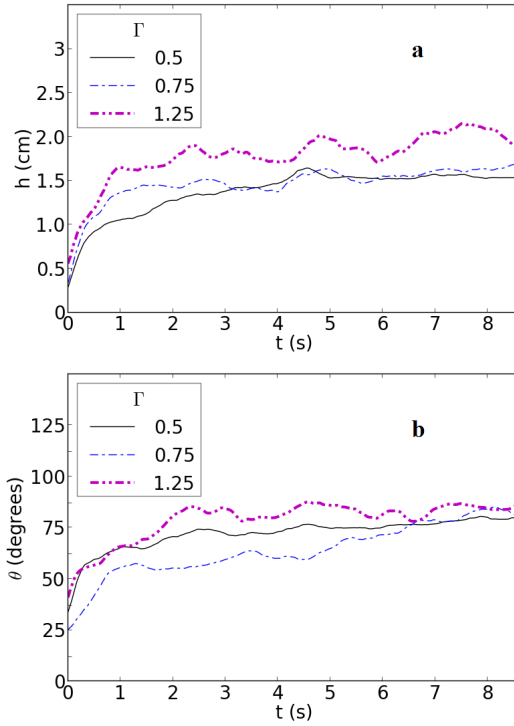


FIG. 12. (color online) Time dependence of sinking depth (a) and tilting angle (b) for a simulated quasi-2D Ring cylinder.

angle is a few tens of degrees, but during the shaking with ring, the intruder tilts fast, reaching a angle between 80 and 90° (see Fig. 5): the intruder almost ends up lying on one of its sides.

An interesting result of the simulations is seen in figure 11 (b): while for the smaller accelerations the tilting angle of the No-ring cylinders oscillate around 0°, for the adimensional acceleration  $\Gamma = 1.25$  the No-ring cylinder reaches an angle of approximately 25°. It suggests that, for big enough accelerations, it is possible to tilt the cylinder, independently of the details of its foundation. Some preliminary experimental results obtained by us using higher frequencies of shaking (which gives higher adimensional accelerations) does confirm that finding.

### Conclusions

In this paper, we have studied the behavior of cylindrical objects as they sink into a dry granular bed fluidized by horizontal oscillations, as a model system to understand the effects of earthquake-related fluidization of soils on human constructions and other objects like rocks.

We have found that, within a relatively large range of lateral shaking amplitudes at a frequency of 5 Hz, cylinders with flat bottoms sink vertically, while those with a “foundation” consisting in a shallow ring attached to their

bottom, tilt laterally besides vertically sink. The tilting is associated to the torque experienced by the cylinder when the ring at the bottom increases the friction with the laterally-accelerated granular bed.

We have been able to mimic the above described behaviors by quasi-2D numerical simulations. We have also reproduced the vertical sink dynamics of cylinders with a flat base using a Newtonian equation of motion for an object penetrating a fluidized layer of granular matter, where the granular effective density increases with depth, eventually reaching a solid phase. The same model allows to understand the sinking even in the present of tilting.

Finally, it is worth noting that preliminary experimental data and quasi-2D numerical simulations suggest that, when strong enough lateral shaking is applied, the tilting scenario tends to dominate regardless the nature of the intruder’s foundation.

### ACKNOWLEDGEMENTS

We acknowledge support from Project 29942WL (Fonds de Solidarité Prioritaire France-Cuba), from the EU ITN FlowTrans, and from the Alsatian network REALISE. E. A. drew inspiration from the late M. Álvarez-Ponte.

- 
- [1] J. D. Bray and J. P. Stewart “Damage patterns and foundation performance in Adapazari, in Kocaeli, Turkey earthquake of August 17, 1999”. Reconnaissance Report, Earthquake Spectra **16** (Suppl. A), 163 (2000).
  - [2] R. B. Sancio, J. D. Bray, J. P. Stewart, T. L. You, H. T. Durgunoglu, A. Onalp, R. B. Seed, C. Christensen, M. B. Baturay and T. Karadayilar, *Soil Dyn. Earthquake Engng.* **22**, 1093 (2002).
  - [3] R. B. Sancio, J. D. Bray, T. Durgunoglu and A. Onalp. Proc. 13th Conference in Earthquake Engineering, Vancouver, B.C., Canada (August 1-6, 2004), Paper No. 935.
  - [4] N. N. Ambraseys, Engineering seismology, Special Issue—the 1987 Mallet-Milne lecture. *J. Earthq. Eng. Struct. Dyn.* **17**, 1 (1988).
  - [5] K. Vanneste, M. Meghraoui and T. Camelbeeck, *Tectonophysics* **309**, 57 (1999).
  - [6] National Research Council, “Liquefaction of Soils During Earthquakes”, (National Academy Press, Washington, DC, 1985).
  - [7] J. B. Berril and R. O. Davis, *Soils Found.* **25**, 106 (1985).
  - [8] E. Clément and J. Rajchenbach, *Europhys. Lett.* **16**, 133 (1991).
  - [9] C. Y. Wang and M. Manga, “Earthquakes and Water” (Springer, Berlin, Heidelberg, 2014).
  - [10] H. Jaeger, S. Nagel and R. Beringer, *Rev. Mod. Phys.* **68**, 1259 (1996).
  - [11] T. Shinbrot and F. J. Muzzio, *Phys. Rev. Lett.* **81**, 4365 (1998).

- [12] E. Altshuler, O. Ramos, E. Martínez, A. J. Batista-Leyva, A. Rivera and K. E. Bassler, *Phys. Rev. Lett.* **91**, 014501 (2003).
- [13] I. S. Aranson and L. S. Tsimring, *Rev. Mod. Phys.* **78**, 641 (2006).
- [14] B. Andreotti, Y. Forterre and O. Pouliquen, “Granular matter: between fluid and solid” (Cambridge University Press, Cambridge, 2013).
- [15] E. Altshuler, R. Toussaint, E. Martínez, O. Sotolongo-Costa, J. Schmittbuhl and K. J. Måløy, *Phys. Rev. E* **77**, 031305 (2008).
- [16] J. F. Boudet, Y. Amarouchene, B. Bonnier and H. Kellay, *Journal of Fluid Mechanics*, **572**, 413 (2007).
- [17] J. L. Vinningland, Ø. Johnsen, E. G. Flekkøy, R. Toussaint and K. J. Måløy, *Phys. Rev. Lett.* **99**, 048001 (2007).
- [18] Ø. Johnsen, R. Toussaint, K. J. Måløy and E. G. Flekkøy, *Phys. Rev. E* **74**, 011301 (2006).
- [19] Ø. Johnsen, C. Chevalier, A. Lindner, R. Toussaint, E. Clément, K. J. Måløy, E. G. Flekkøy and J. Schmittbuhl, *Phys. Rev. E* **78**, 051302 (2008).
- [20] M. J. Niebling, E. G. Flekkøy, K. J. Måløy and R. Toussaint, *Phys. Rev. E* **82**, 051302 (2010).
- [21] M. J. Niebling, E. G. Flekkøy, K. J. Måløy and R. Toussaint, *Phys. Rev. E* **82**, 011301 (2010).
- [22] M. J. Niebling, R. Toussaint, E. G. Flekkøy and K. J. Måløy, *Phys. Rev. E* **86**, 061315 (2012).
- [23] S. Turkaya, R. Toussaint, F. K. Eriksen, M. Zecevic, G. Daniel, E. G. Flekkøy and K. J. Måløy, *Frontiers in Physics* **3**, 70 (2015).
- [24] J. S. Uehara, M. A. Ambroso, R. P. Ojha and D. J. Durian, *Phys. Rev. Lett.* **90**, 194301 (2003).
- [25] J. F. Boudet, Y. Amarouchene and H. Kellay, *Phys. Rev. Lett.* **96**, 158001 (2006).
- [26] H. Katsuragi and D. Durian, *Nat. Phys.* **3**, 420 (2007).
- [27] D. I. Goldman and P. Umbanhowar, *Phys. Rev. E* **77**, 021308 (2008).
- [28] F. Pacheco-Vázquez, G. A. Caballero-Robledo, J. M. Solano-Altamirano, E. Altshuler, A. J. Batista-Leyva and J. C. Ruiz-Suárez, *Phys. Rev. Lett.* **106**, 218001 (2011).
- [29] L. Kondic, X. Fang, W. Losert, C. S. O’Hern and R. P. Behringer, *Phys. Rev. E* **85**, 011305 (2012).
- [30] H. Torres, A. González, G. Sánchez-Colina, J. C. Drake and E. Altshuler, *Rev. Cub. Fis.* **29**, 1E45 (2012).
- [31] A. H. Clark and R. P. Behringer, *Europhys. Lett.* **101**, 4001 (2013).
- [32] J. C. Ruiz-Suárez, *Rep. Prog. Phys.* **76**, 066601 (2013).
- [33] T. A. Brzinski III, P. Mayor and D. J. Durian, arXiv: 1307.4638 [cond-mat.soft] (2013).
- [34] E. Altshuler, H. Torres, A. González-Pita, G. Sánchez-Colina, C. Pérez-Penichet, S. Waitukaitis and R. C. Hidalgo, *Geophys. Res. Lett.* **41**, 3032 (2014).
- [35] R. Harich, T. Darnige, E. Kolb and E. Clément, *Europhys. Lett.* **96**, 54003 (2011).
- [36] E. Kolb, J. Cviklinski, J. Lanuza, P. Claudin and E. Clément, *Phys. Rev. E* **69**, 031306 (2004).
- [37] S. Joubaud, T. Homan, Y. Gasteuil, D. Lohse and D. van der Meer, *Phys. Rev. E* **90**, 060201(R) (2014).
- [38] G. Metcalfe, S. G. K. Tennakoon, L. Kondic, D. G. Schaeffer and R. P. Behringer, *Phys. Rev. E* **65**, 031302 (2002).
- [39] Ch. A. Kruehle, *Rev. Adv. Mater. Sci.* **20**, 113 (2009).
- [40] S. G. K. Tennakoon, L. Kondic, R. P. Behringer, *Europhys. Lett.* **45**(4), 470 (1999).
- [41] H. Liu and R. Dobry, *J. Geotechnical and Geoenvironmental Engng.* **123**, 557 (1997).
- [42] G. Sánchez-Colina, L. Alonso-Llanes, E. Martínez, A. J. Batista-Leyva, C. Clément, C. Flidner, R. Toussaint and E. Altshuler *Rev. Sci. Inst.* **85**, 126101 (2014).
- [43] P. A. Cundall and O. D. Strack. A discrete numerical model for granular assemblies. *Geotechnique*, Ice Virtual Library, **29**, 47 (1979).
- [44] S. Parez, E. Aharonov and R. Toussaint, *Phys. Rev. E* **93**, 042902 (2016).
- [45] R. Toussaint, C. Clément, C. Flidner, M. Stojanova, E. Aharonov, G. Sanchez-Colina, E. Altshuler, A. J. Batista-Leyva and E. G. Flekkøy, *Geophysical Research Abstracts* **16** EGU2014, 12539, (2014).
- [46] J. R. de Bruyn and A. M. Walsh, *Can. J. Phys.* **82**, 439 (2004).
- [47] M. Hou, Z. Peng, R. Liu, Y. Wu, Y. Tian, K. Lu and C. K. Chan, *Sci. Tech. Adv. Mat.* **6**, 855 (2005).
- [48] X. Zhang, D. Sheng, G. P. Kouretzis, K. Krabbenhoft and S. W. Sloan, *Phys. Rev. E* **91**, 022204 (2015).